High-Temperature Raman Spectroscopy of UCl3 : A Combined Experimental and Theoretical Study

Strzelecki, Andrew Charles; Wang, Gaoxue; Hickam, Sarah Margaret; Parker, Stephen Scott; Batrice, Rami John; Jackson, Jay Matthew; Conroy, Nathan Alec; Mitchell, Jeremy Neil; Andersson, Anders David Ragnar; Monreal, Marisa Jennifer; Boukhalfa, Hakim; Xu, Hongwu

To be published in: Inorganic Chemistry

DOI to publisher's version: 10.1021/acs.inorgchem.3c03139

Inorganic Chemistry

pubs.acs.org/IC

Article

In Situ High-Temperature Raman Spectroscopy of UCl_3: A Combined Experimental and Theoretical Study

Andrew C. Strzelecki, Gaoxue Wang, Sarah M. Hickam, S. Scott Parker, Rami Batrice, J. Matt Jackson, Nathan A. Conroy, Jeremy N. Mitchell, David A. Andersson, Marisa J. Monreal, Hakim Boukhalfa, and Hongwu Xu*

Cite This: https://doi.org/10.1021/acs.inorgchem.3c03139

Read Online

ACCESS | Metrics & More | Article Recommendations | Supporting Information

ABSTRACT: Uranium trichloride (UCl_3) has received growing interest for its use in uranium-fueled molten salt reactors and in the pyrochemical processing of used fuel. In this paper, we report for the first time the experimentally determined Raman spectra of UCl_3, at both ambient condition and *in situ* high temperatures up to 871 K. The frequencies of five of the Raman-active vibrational modes (ν_i) of UCl_3 exhibit a negative temperature derivative ($(\partial\nu_i/\partial T)_P$) with increasing temperature. This red-shift behavior is likely due to the elongation of U−Cl bonds. The average isobaric mode Grüneisen parameter ($\gamma_{iP} = 0.91 \pm 0.02$) of UCl_3 was determined through use of the coefficient of thermal expansion published in Vogel et al. (2021) and the $(\partial\nu_i/\partial T)_P$ values determined in this study. These results are in general agreement with those calculated here by density functional theory (DFT+U). Finally, a comparison of the ambient band positions of UCl_3 to those of isostructural lanthanide (La−Eu) and actinide chlorides (Am−Cf) has been made.

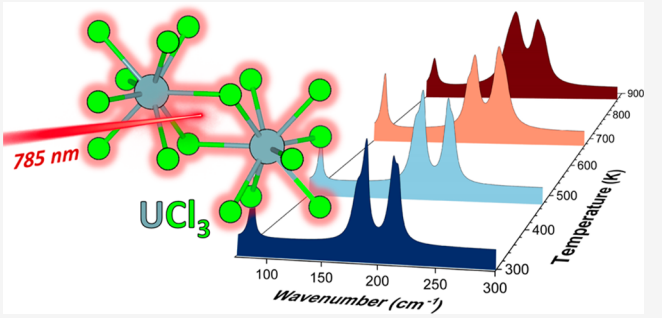

1. INTRODUCTION

Growth in nuclear power is anticipated as an environmentally conscious, carbon-free energy source. A significant problem encountered with the light water reactors (LWRs) of generation II and III nuclear power plants is, however, that they generate transuranium byproducts. These byproducts are often the longest lived radioisotopes[1] and of the greatest concern from the perspective nonproliferation. Hence, these radioelements have been a significant focus in nuclear waste disposal strategies.[2−4] Conventionally, the disposal strategy of such wastes is through either a mined geological repository or a deep drilled borehole.[5−7] Another approach of dealing with the generation of nuclear waste is to design a nuclear reactor that can utilize more of the input fuel and consume the transuranium elements. This would significantly decrease the amount of radioactive waste produced and increase the environmental benefits of the carbon-free nuclear power. In the generation IV nuclear power plant designs, molten salt reactors (MSRs) have all these attributes. An example of such a reactor is at the Accelerator Research Laboratory (ARL), Texas A&M University (TAMU), where a method for accelerator-based destruction of actinides in molten salt (ADAM) to burn transuranium elements has been developed.[8] Although most of the research on MSR technologies has been toward fluoride-based fuel salts,[9−11] chloride-based fuel salts have higher solubility for actinides, can operate at lower temperatures, and have higher volumetric heat capacity, while possessing good thermal conductivity and low viscosity.[12−16] All of these properties make chloride-based MSRs ideal for burning transuranium elements.[12,13] Despite this, there are still considerable knowledge gaps in the structures and properties of chloride salts at high temperatures.

Uranium trichloride (UCl_3) is of significant interest as a fuel in MSRs. Recent advances have been made through a combination of both experimental (neutron scattering, neutron imaging, calorimetry, and dilatometry)[15,17,18] and computational (density functional theory)[19] methods. UCl_3 is a prototypical compound, crystallizing in the hexagonal $P6_3/m$ structure,[20] and nearly 100 other isostructural compounds have been reported in the Inorganic Crystal Structure Database (ICSD).[18] However, despite the importance of this phase, its Raman spectrum, to the best of our knowledge, has not been reported in the literature. In this study, we conducted first-ever Raman spectroscopic measurements of UCl_3 from 298 to 871 K. Five Raman-active modes of UCl_3 have been revealed, and

Received: September 7, 2023
Revised: October 18, 2023
Accepted: October 19, 2023

the variations of their frequencies as a function of temperature have been determined. The obtained results were validated by density functional theory (DFT) calculations. Furthermore, these results allowed us to determine the isobaric mode Grüneisen parameters (γ_{iP}) of the five Raman modes of UCl_3.

2. EXPERIMENTAL METHODS

2.1. Sample Preparation. Because UCl_3 is very hygroscopic and is subjected to oxygen pollution in air, all sample preparation was done in an inert argon atmosphere drybox, where the O_2 and moisture levels were monitored and maintained at ≤1 ppm. UCl_3 was synthesized from uranium metal by conversion to hydride (UH_3) and subsequent chlorination to UCl_3.[21] The phase purity of UCl_3 was verified by powder X-ray diffraction and melt point analysis via differential scanning calorimetry, the details of which are presented in our earlier works.[17,18] A UCl_3 powder sample (<5 mg) was placed in a silica (SiO_2) capillary (Technical Glass Inc.), which was approximately 8 mm in length, with a 1 mm inner diameter, a 2 mm outer diameter, and had a wall thickness of 0.5 mm. The capillary containing UCl_3 was transferred out of the argon atmosphere drybox under vacuum, and the other end of the capillary was then sealed with an Arizona Hydrogen Flame Generator MG-300 H_2−O_2 torch.

2.2. Raman Spectroscopy. Raman spectroscopic measurements were performed using a Horiba LabRAM HR Evolution microscope equipped with an Olympus 5× objective in backscattering/reflection mode. The instrument was calibrated with a silicon wafer using the first-order Si line at 520.7 cm^{-1}. The measurements were conducted by using a TOPTICA Photonics 785 nm diode laser to avoid the fluorescence signals, which would be present in the Raman spectra collected using a lower wavelength laser (e.g., 532 nm). The maximum output of the 785 nm laser is 300 mW. The laser outputs were filtered to 50% of the maximum power (150 mW). The system is equipped with a grating of 600 grooves/mm, which yields an effective resolution of <1 cm^{-1}. Raman spectra of the vibrational bands of UCl_3 were collected from 70 to 300 cm^{-1}. Each spectrum is the result of three accumulations per window with the time of each accumulation being between 30 and 120 s. The total time of counting for each spectrum was approximately 5−20 min, depending on the counting time. Additionally, to verify that no U−O vibrational modes were present at frequencies >300 cm^{-1}, a set of spectra were collected from 300 to 1000 cm^{-1} at 298, 473, 672, and 871 K. The above Raman spectroscopic measurement procedures using the same instrument have been described previously.[22−24]

For *in situ* high-temperature Raman spectroscopic measurements, the capillary containing UCl_3 was placed in a Linkam TS1500 heating stage, and the temperature was increased from room temperature to 871 K (Figure S1). The heating rate was 10 K/min, and a thermal equilibration period of at least 5 min was adopted prior to recording a Raman spectrum at each temperature. Above 871 K, the quality of the collected Raman spectra diminished, and no vibrational bands of UCl_3 could be observed. This loss in signal was due to the emitted electromagnetic radiation of the ceramic heating crucible of the Linkam TS1500 stage, and thus, 871 K was selected as the upper temperature limit for our measurements.

The temperature of the heating stage was calibrated against the α to β transition temperature of quartz (SiO_2; $T_{\alpha-\beta}$ = 847.5 K). The same heating rate (10 K/min) and thermal equilibration period (5 min) as for UCl_3 measurements were used. For these calibration measurements, a single crystal of high purity natural quartz (Hot Springs, Arkansas) was powdered with an agate mortar and pestle, and the powders were placed into the heating stage on a sapphire window. The α to β quartz transition was deemed complete once the A_1 mode at 355 cm^{-1} disappeared.[25] This was done by thermally cycling the quartz sample above (871 K) and below (836 K) the transition temperature (847.5 K)[26] several times. The Raman spectroscopic measurements for the temperature calibration were done with the same Horiba system but used a 532 nm Nd:YAG laser. The maximum output of the 532 nm laser is 200 mW. The laser outputs were filtered to 50% of the maximum power (100 mW). Raman spectra of the vibrational bands of quartz were collected from 70 to 600 cm^{-1}. Each spectrum is the result of three accumulations per window with the time of each accumulation being between 10 and 30 s. The total time of counting for each spectrum was approximately 5 min.

2.3. Density Functional Theory Calculations. Our calculations were performed with the use of density functional theory (DFT) and projector augmented-wave (PAW) method[27] as implemented in the Vienna Ab initio Simulation Package (VASP).[28] The Perdew−Burke−Ernzerhof (PBE)[29] functional of generalized gradient approximation (GGA) was used to represent the exchange−correlation interaction. The van der Waals (vdW) interaction was included in the calculations with the DFT-D3 method of Grimme.[30] A Γ-centered 7 × 7 × 13 k-point grid and plane-wave cutoff energy of 500 eV were employed for structural optimization.[27] The energy convergence was set to 10^{-6} eV, and the residual force on each atom was less than 0.01 eV/Å. A Hubbard on-site correction of 4.0 eV was applied on the 5*f* orbitals of uranium atoms.[31,32] The predicted lattice constants of UCl_3 are a = 7.40 Å and c = 4.31 Å.

The Phonopy code[33] was employed to compute the vibrational frequencies. The input force constants for Phonopy were derived using density functional perturbation theory (DFPT)[34] employing a 1 × 1 × 2 supercell. To assess the temperature-dependent behavior of the vibrational frequencies, the thermal expansion of UCl_3 was analyzed across various temperatures using the quasi-harmonic approximation (QHA).[18,35] The free energy as a function of volume at each temperature and therefore the equilibrium volume as a function of temperature were obtained from the vibrational free energy and the equation of states at 0 K.

3. RESULTS

The crystal structure of UCl_3 possesses a hexagonal symmetry with the $P6_3/m$ space group and C_{6h} point group.[20] The unit cell contains two formula units.[20,36] U^{3+} is 9-fold coordinated to Cl^-, creating the [UCl_9] polyhedron with a tricapped trigonal prismatic geometry (Figure 1).[37] Factor group analysis of this space group predicts the occurrence of six Raman-active bands, $\Gamma_{Raman} = 2A_g + E_g + 3E_{2g}$.[36] While the A_g mode corresponds to the motion of Cl^- in the *ab*-plane of the structure (Figure 1a), the E_{1g} mode corresponds to the Cl^- motion out of the *ab*-plane along the *c*-axis (Figure 1b).[36] The E_{2g} mode can be classified as a translational mode of the U^{3+} and Cl^- ions that move together parallel to the *ab*-plane.[36]

Band component analysis of the UCl_3 Raman spectra was made by means of the Peakfit function within the OriginPro 2021 software suite. The background of each spectrum was determined using the second-derivative method with up to 20 anchor points that were connected by nonlinear interpolation of a B-spline function.[38] The peaks were fitted using a Lorentz function with the minimum number of components.[38] The raw uncorrected spectra are presented in the electronic supplement (Figure S3). A total of 12 temperature-dependent Raman spectra were deconvoluted. A representative deconvolution is shown in Figure 2. The adjusted R^2 values from the fits range from 0.971 to 0.993, with a mean adjusted R^2 of 0.986. The results from deconvolutions are listed in Table 1. At ambient conditions, the Raman spectrum of UCl_3 has five bands at 83.6, 178.7, 186.1, 210.3, and 215.5 cm^{-1} (Table 1). Based on our DFT calculations (see below), the Raman bands of UCl_3 can be assigned as follows: the vibrational bands at 83.6 and 215.5 cm^{-1} correspond to the E_{2g} mode, the bands at 178.7 and 210.3 cm^{-1} belong to the A_g mode, and the 186.1 cm^{-1} band corresponds to the E_{1g} mode. It is predicted that there exists a sixth Raman mode (E_{2g}), but its intensity is too low to be detected.[39] The observed Raman modes and assignments are in good accordance with those of the previously studied

https://doi.org/10.1021/acs.inorgchem.3c03139
Inorg. Chem. XXXX, XXX, XXX−XXX

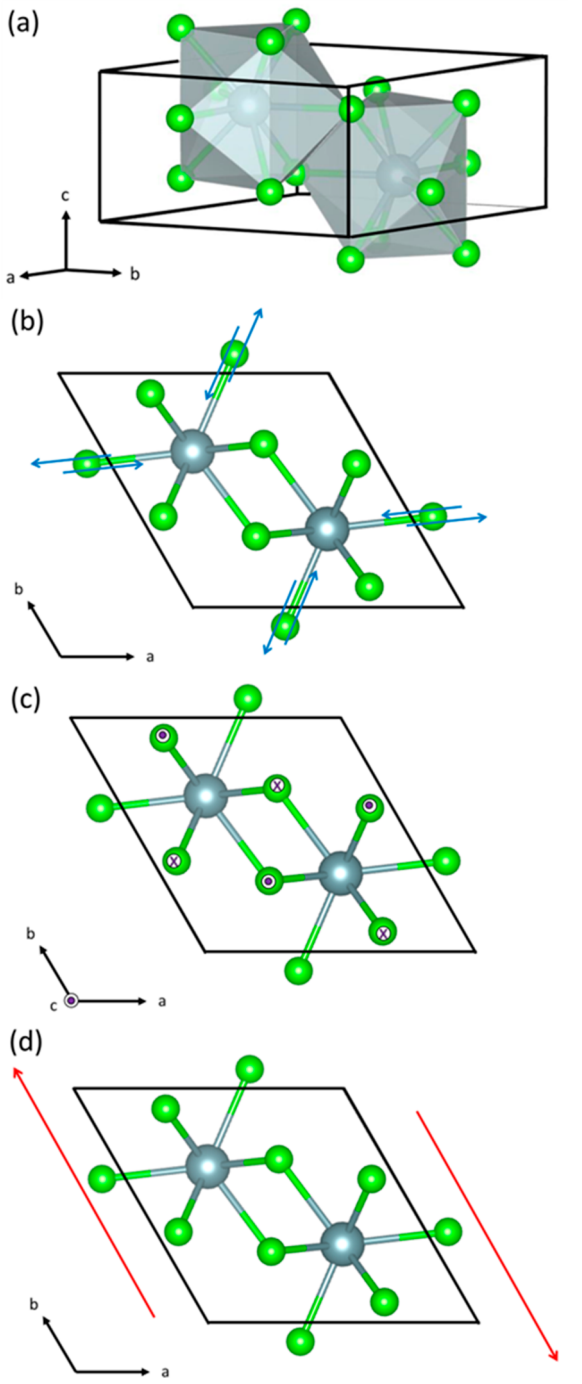

Figure 1. Visualization of the Raman-active modes of UCl_3. (a) depicts how U^{3+} is 9-fold coordinated to Cl^-, creating the $[UCl_9]$ polyhedron with a tricapped trigonal prismatic geometry. (b) depicts the A_g mode and how the Cl^- ion moves parallel to (blue arrow) the *ab*-plane. (c) depicts the E_g mode and how the Cl^- ion moves in (purple dot) and out (purple x) along the *c*-axis; and (d) depicts the E_{2g} mode and how the U^{3+} and Cl^- ions translationally move together (red arrow) parallel to the *ab*-plane.[67]

isostructural lanthanide ($LnCl_3$, where Ln = La, Ce, Pr, Pm, Sm, Eu, Gd) and actinide ($AnCl_3$, where An = Am, Cm, Cf) trichlorides.[36,37,40−46]

It was found that the capillary sealing methodology successfully prevented degradation of the UCl_3 sample via oxidation and/or hydration (Figure S4). This was evident, as there are no U−O vibrational modes present in any of the

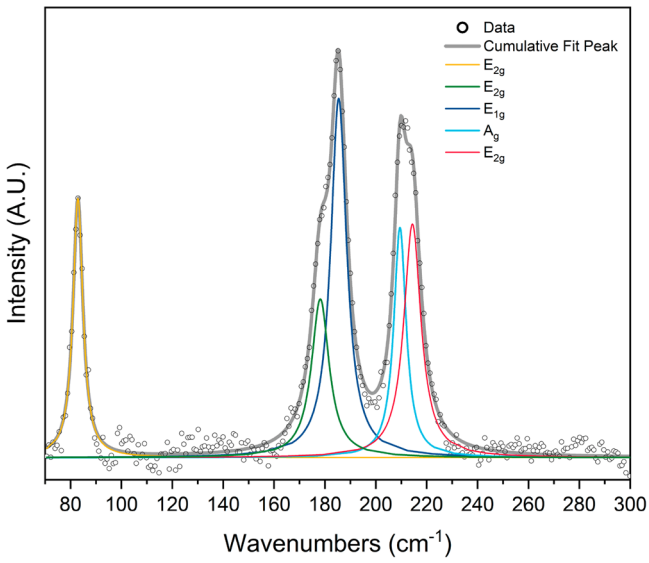

Figure 2. Representative deconvolution of a background subtracted Raman spectrum of UCl_3 recorded at 298 K. The adjusted R^2 of the deconvolution is 0.988.

spectra that were recorded between 300 and 1000 cm^{-1}; in uranium oxychloride (UO_2Cl_2), there is a strong temperature-dependent vibrational band located between 700 and 760 cm^{-1}.[47] Additionally, there are no vibrational features near 450 cm^{-1}, which occurs in uranium dioxide $[(U^{4+}O_2)^0]$, and near 775 cm^{-1}, which occurs in uranyl $[(U^{6+}O_2)^{2+}]$ hydrates and oyxhydrates.[48−50]

Our DFT calculations indicated that there are six Raman-active modes as well as three infrared (IR)-active modes (Figure S2). At 0 K, the DFT predicted Raman spectrum of UCl_3 would exhibit bands at 73.6, 158.4, 168.3, 174.7, 201.6, and 204.5 cm^{-1} (Table 2). The band assignments are as follows: the vibrational bands at 73.6, 158.4, and 204.5 cm^{-1} correspond to the E_{2g} mode, the bands at 168.3 and 201.6 cm^{-1} belong to the A_g mode, and the 174.7 cm^{-1} band corresponds to the E_{1g} mode. Note that the E_{2g} mode at 158.4 cm^{-1} was not observed experimentally, probably because its intensities were below the detection limit. In addition, there are three infrared (IR)-active modes at 126.4, 132.6, and 187.7 cm^{-1}. The IR band at 126.4 cm^{-1} is assigned to the A_u mode, while those at 132.6 and 187.7 cm^{-1} are assigned to the E_{1u} mode. These IR-active modes need experimental verification by far-IR spectroscopy.

4. DISCUSSION

4.1. Vibrational and Bonding Characteristics of UCl_3.

Our experimental and computational results show that all of the Raman bands (Figures 3 and 4) exhibit a red-shift with increasing temperature. These thermally induced frequency shifts are likely a result of the lengthening of the U−Cl bonds in the structure of UCl_3. There was no emergence or disappearance of vibrational bands in the temperature range investigated, suggesting no apparent phase transitions. This observation of no apparent phase transitions is consistent with the previous high-temperature neutron diffraction and differential scanning calorimetry experiments.[17,18] The variations of vibrational frequencies for all measurable Raman modes with temperature are illustrated in Figure 4. All of the vibrational modes systematically exhibit a negative temperature depend-

https://doi.org/10.1021/acs.inorgchem.3c03139
Inorg. Chem. XXXX, XXX, XXX−XXX

Table 1. Raman Band Positions of UCl_3 from 298 to 871 K Obtained from Deconvolutions of *In Situ* High-Temperature Raman Spectra

temp (K)	E_{2g} (cm^{-1})	A_g (cm^{-1})	E_{1g} (cm^{-1})	A_g (cm^{-1})	E_{2g} (cm^{-1})	adj R^2
298	83.6 ± 0.1	178.7 ± 0.2	186.1 ± 0.1	210.3 ± 0.1	215.4 ± 0.2	0.990
348	83.3 ± 0.1	178.6 ± 0.3	185.5 ± 0.1	209.9 ± 0.2	215.4 ± 0.3	0.987
398	82.9 ± 0.1	178.2 ± 0.3	185.0 ± 0.1	209.4 ± 0.2	215.0 ± 0.7	0.989
448	82.4 ± 0.1	177.2 ± 0.3	184.4 ± 0.2	208.8 ± 0.3	214.4 ± 0.7	0.991
522	81.9 ± 0.1	176.3 ± 0.4	183.7 ± 0.2	208.1 ± 0.2	214.2 ± 0.4	0.993
572	81.6 ± 0.1	176.0 ± 0.3	183.2 ± 0.2	207.7 ± 0.2	214.0 ± 0.5	0.987
622	81.3 ± 0.1	175.6 ± 0.4	183.0 ± 0.3	207.2 ± 0.3	213.7 ± 0.6	0.986
672	80.9 ± 0.1	174.1 ± 0.4	181.7 ± 0.3	207.1 ± 0.4	214.6 ± 0.9	0.984
722	80.7 ± 0.1	173.1 ± 0.5	181.0 ± 0.3	206.0 ± 0.4	212.3 ± 0.6	0.986
772	81.1 ± 0.1	173.5 ± 0.4	180.9 ± 0.3	205.2 ± 0.3	212.1 ± 0.4	0.984
822	80.3 ± 0.1	172.2 ± 0.5	180.2 ± 0.4	204.8 ± 0.5	211.5 ± 0.7	0.985
871	79.7 ± 0.1	169.9 ± 1.7	179.8 ± 0.8	205.3 ± 0.6	214.3 ± 1.0	0.985

Table 2. Raman Band Positions of UCl_3 from 0 to 800 K Predicted by DFT Calculations

temp (K)	E_{2g} (cm^{-1})	A_g (cm^{-1})	E_{1g} (cm^{-1})	A_g (cm^{-1})	E_{2g} (cm^{-1})
0	73.6	158.4	168.3	174.7	201.6
200	71.8	153.8	162.4	172.3	197.3
400	70.0	147.7	159.1	170.6	192.4
600	67.7	141.9	156.0	169.2	188.2
800	63.5	137.2	151.7	167.2	183.0

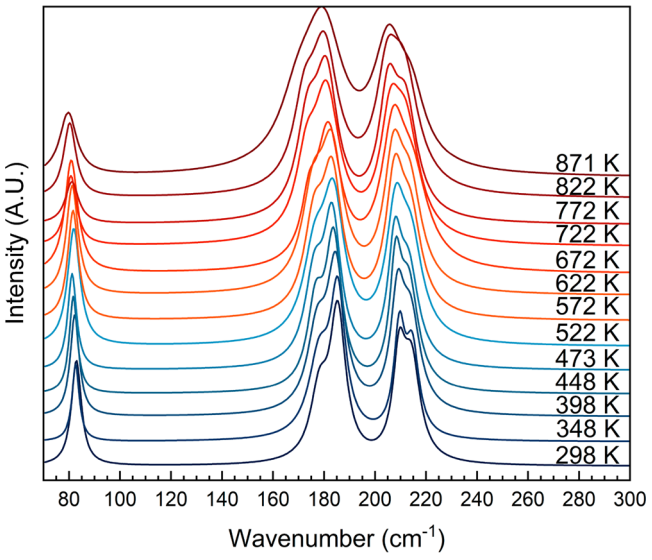

Figure 3. Selected Raman spectra of UCl_3 from 298 to 871 K. The presented spectra are the cumulative fits resulting from the deconvolutions at different temperatures.

ency by means of a linear regression, $\upsilon_i = a_i + b_iT$. The fitted temperature coefficients (b_i) of the Raman modes are listed in Table 3.

The Grüneisen parameter (γ) is a dimensionless quantity which is useful in quantifying the relationship between the thermal and elastic properties of a solid.[51] The temperature coefficients (b_i) of the Raman modes (Table 3) can be utilized to calculate the isobaric mode Grüneisen parameter (γ_{iP}), as it is equivalent to $\left(\frac{\partial \nu_i}{\partial T}\right)_P$ through the following relationship:

$$\gamma_{iP} = \left(-\frac{1}{\alpha \nu_i}\right)\left(\frac{\partial \nu_i}{\partial T}\right)_P \quad (1)$$

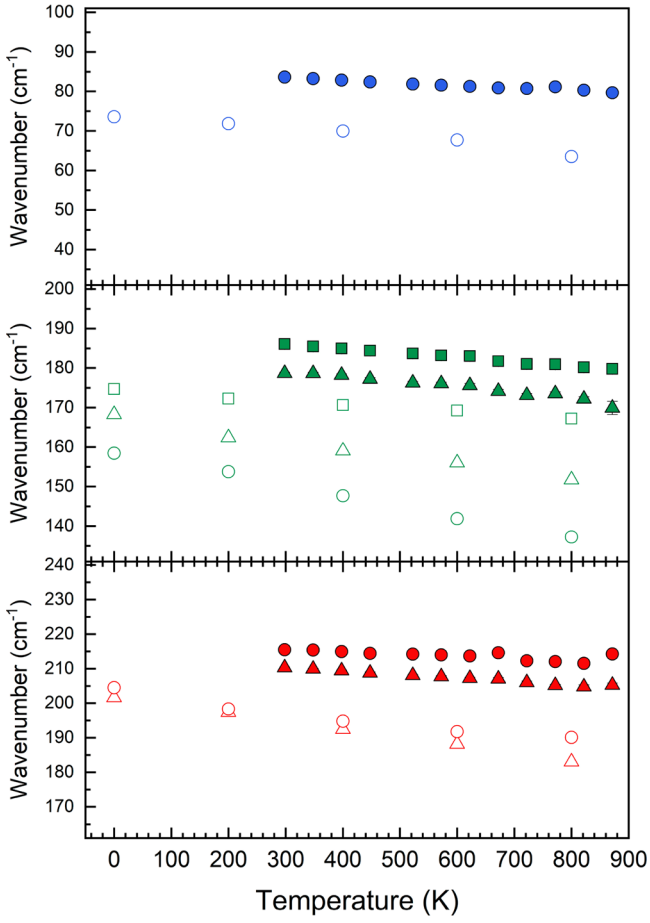

Figure 4. Variation of the frequencies of Raman modes of UCl_3 with temperature determined experimentally and computationally. Circles indicate the E_{2g} modes, squares indicate the E_{1g} mode, and triangles indicate the A_g modes. Shaded shapes are experimentally determined values, and hollow shapes are computationally determined values.

where υ_i is the vibrational frequency of the ith vibrational band and α is the isobaric thermal expansion coefficient, which is defined by $\alpha = \left(\frac{1}{V}\right)\left(\frac{\partial V}{\partial T}\right)_P$. The isobaric thermal expansion of UCl_3 was determined by Vogel et al., using *in situ* high-temperature neutron diffraction, to be $(6.32 \pm 0.16) \times 10^{-5}$ K^{-1}[18] and was used in the derivation of the γ_{iP} (Table 3). The average value of γ_{iP} for UCl_3 was found to be 0.91 ± 0.02.

https://doi.org/10.1021/acs.inorgchem.3c03139
Inorg. Chem. XXXX, XXX, XXX−XXX

Table 3. Fitted Parameters a and b in $\upsilon_i = a_i + b_iT$ from the Frequencies (υ_i) of High-T Raman Bands of UCl_3 and the Determined Isobaric Mode Grüneisen Parameters (γ_{iP})

parameter	E_{2g}	A_g	E_{1g}	A_g	E_{2g}
a_i (cm^{-1})	83.70 ± 0.07	179.4 ± 0.2	186.37 ± 0.06	210.63 ± 0.08	215.7 ± 0.2
b_i (cm^{-1}/K)	−0.0068 ± 0.0003	−0.0124 ± 0.0007	−0.0111 ± 0.0003	−0.0101 ± 0.0003	−0.0064 ± 0.0008
adj R^2	0.982	0.964	0.993	0.988	0.858
γ_{iP}	1.29 ± 0.06	1.10 ± 0.07	0.94 ± 0.03	0.75 ± 0.03	0.46 ± 0.06

Table 4. Force Constants of the Raman Modes of UCl_3

temp (K)	E_{2g} (N/m)	E_{2g} (N/m)	E_{1g} (N/m)	A_{1g} (N/m)	E_{2g} (N/m)
298	12.72 ± 0.01	58.04 ± 0.08	62.97 ± 0.03	80.42 ± 0.05	84.42 ± 0.09
348	12.61 ± 0.01	58.02 ± 0.08	62.55 ± 0.04	80.12 ± 0.06	84.33 ± 0.12
398	12.49 ± 0.01	57.74 ± 0.10	62.22 ± 0.05	79.74 ± 0.06	84.01 ± 0.12
448	12.35 ± 0.01	57.10 ± 0.11	61.83 ± 0.06	79.25 ± 0.11	83.60 ± 0.28
522	12.19 ± 0.01	56.48 ± 0.11	61.34 ± 0.06	78.71 ± 0.08	83.43 ± 0.16
572	12.10 ± 0.01	56.35 ± 0.11	61.00 ± 0.07	78.46 ± 0.09	83.26 ± 0.18
622	12.01 ± 0.01	56.07 ± 0.14	60.90 ± 0.10	78.09 ± 0.12	83.03 ± 0.21
672	11.90 ± 0.01	55.14 ± 0.13	60.03 ± 0.09	77.97 ± 0.14	83.72 ± 0.34
722	11.85 ± 0.02	54.48 ± 0.15	59.57 ± 0.10	77.15 ± 0.16	81.94 ± 0.25
772	11.97 ± 0.04	54.74 ± 0.14	59.52 ± 0.10	76.56 ± 0.11	81.77 ± 0.17
822	11.72 ± 0.02	53.91 ± 0.17	59.01 ± 0.13	76.25 ± 0.19	81.36 ± 0.28
871	11.54 ± 0.03	52.48 ± 0.51	58.77 ± 0.27	76.61 ± 0.22	83.46 ± 0.38

The bond force constant (k) represents the interaction between nearest atoms and is determined by both the length and angle of the bond. This constant is useful in the analysis of the lattice dynamics. A simplified way of approximating the bond force constant (k) is through use of the Hooke's law:[52]

$$k = (2\pi c\upsilon_i)^2\mu \quad (2)$$

where υ_i is the vibrational frequency of the ith vibrational band, c is the velocity of light in a vacuum (2.998×10^{10} cm/s), and μ is the reduced mass of the vibrating atoms (e.g., U and Cl). Using eq 2, we calculated the k values of UCl_3 as a function of temperature (Table 4). For all of the vibrational bands, the force constants were found to decrease with increasing temperature (Table 4). This behavior is probably due to the elongation of U−Cl bonds in the structure. This elongation results in decreases in the electronegative forces between the U^{3+} cation and Cl^- anion, thereby weakening the U−Cl bonds.

4.2. Systematics in the Vibrational Properties of Isostructural Trichlorides. As stated in the Introduction, UCl_3 is the prototypical structure of nearly 100 compounds reported in the ICSD that include eight $LnCl_3$ (Ln = La−Gd) and eight $AnCl_3$ (An = UCl_3−$EsCl_3$) phases.[18] However, despite the importance of this structure, its Raman spectrum has not been reported until this study. Furthermore, it is interesting to compare the vibrational properties of UCl_3 with those of other isostructural lanthanide ($LnCl_3$, where Ln = La, Ce, Pr, Pm, Sm, Eu, Gd) and actinide ($AnCl_3$, where An = Am, Cm, Cf) trichlorides.[36,37,40−46]

Many physical and chemical properties of isostructural inorganic materials can be evaluated through various empirically derived relationships.[53−62] These relationships link a specific property variable to a structural parameter of the isostructural phases and allow the study of the systematics of the said variable. One of these relationships would be looking at how the frequency of the Raman band changes across isostructural $LnCl_3$ and $AnCl_3$. As Raman spectroscopy is a type of vibrational spectroscopy, the positions of the vibrational bands are sensitive to changes in the reduced mass (μ) and bond length.[52,63,64] Plotting the published vibrational band positions[36,37,40−46] of the $LnCl_3$ and $AnCl_3$ compounds against either the ionic radii (Figure 5a) or μ (Figure 5b) of the trivalent f-metal center in a 9-fold coordination environment allows for determination of any systematic trend.[65,66]

The vibrational frequencies of Raman bands for all of the isostructural f-metal trichlorides, apart from the low-frequency E_{2g} mode, show near-linear dependencies with ionic radii (Figure 5a), where the smaller cations (i.e., Gd^{3+}, Eu^{3+}, and Cf^{3+}) have higher wavenumbers than larger cations (i.e., La^{3+}, Ce^{3+}, and U^{3+}). This suggests that the vibrational modes of these f-metal trichlorides are strongly influenced by lengths of the f-metal−chlorides bonds. One exception is that the low-frequency E_{2g} modes of $LnCl_3$ and $AnCl_3$ display two independent trends with respect to ionic radii (Figure 5a). Instead, the low-frequency E_{2g} mode shows a stronger dependency with μ (Figure 5b), illustrating the strong influence that mass has on vibrational properties.

In terms of similarity in Raman spectra to the other isostructural metal trichlorides, UCl_3 is most like $CeCl_3$ and $AmCl_3$. The ionic radii of U^{3+} (1.189 Å)[66] and Ce^{3+} (1.196 Å)[65] are very similar (<0.60% difference). As a result, the frequencies for four of the five Raman-active modes of UCl_3 and $CeCl_3$ differ only by a maximum of 1.3%. On the other hand, the positions for the low-frequency E_{2g} mode of UCl_3 and $CeCl_3$ are dissimilar, as this mode is more affected by the mass of the metal center than the ionic radii (Figure 5b). Here UCl_3 is most like $AmCl_3$, as the two metal centers are closer in atomic mass to one another than U is to Ce. One would expect that overall the Raman spectrum of UCl_3 to be most similar to those of $NpCl_3$ and $PuCl_3$ because both the atomic masses of the metal centers and the ionic radii in a 9-fold coordination (Np^{3+} = 1.178 Å and Pu^{3+} = 1.168 Å)[66] are closer to one another. However, the Raman spectra of both $NpCl_3$ and $PuCl_3$ have not yet been reported in the literature, and a comparison cannot be made at this time.

https://doi.org/10.1021/acs.inorgchem.3c03139
Inorg. Chem. XXXX, XXX, XXX−XXX

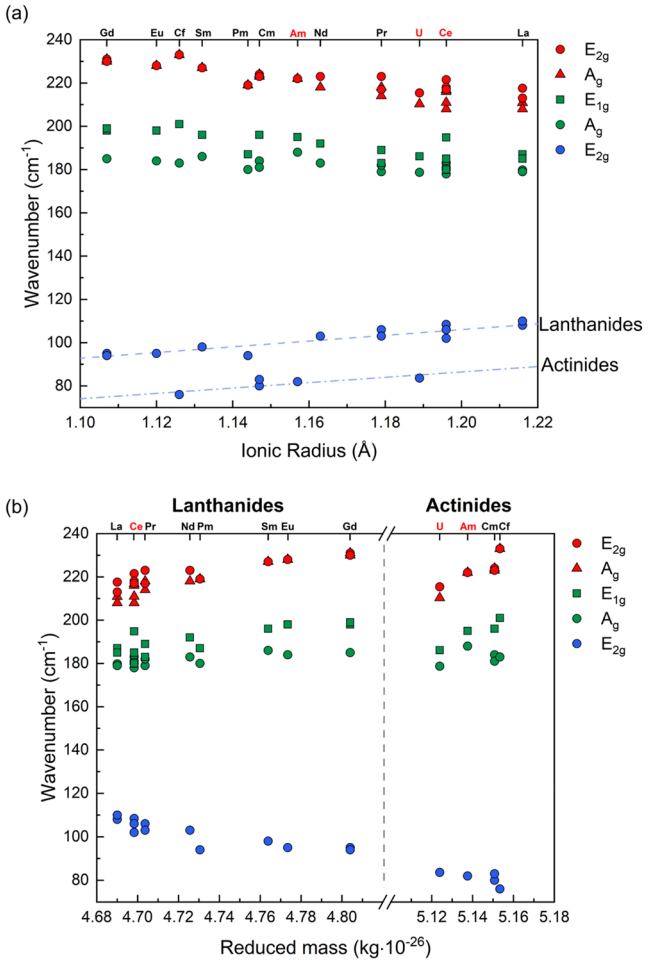

Figure 5. Variation of the frequencies of Raman bands of $LnCl_3$ and $AnCl_3$ as a function of (a) ionic radius and (b) reduced mass of trivalent cation possessing 9-fold coordination.[7,8,10−16,34,35]

5. CONCLUSIONS

Raman spectroscopic measurements of crystalline UCl_3 have been performed from 298 to 871 K, and the obtained results are in general agreement with those predicted by our DFT calculations. This work represents the first Raman spectroscopic study of UCl_3 at both ambient and high temperatures. The band positions of UCl_3 are comparable to those of $CeCl_3$, which possesses a similar ionic radius, and $AmCl_3$, which possesses a similar molecular mass. The frequencies (ν_i) of all five Raman-active modes were determined by deconvoluting the spectra using a Lorentz function. With increasing temperature, all five of the Raman-active vibrational modes exhibit a shift toward lower wavenumbers. This behavior is likely due to the lengthening of U−Cl bonds, which in turn causes a negative temperature derivative in vibrational frequency. The isobaric mode Grüneisen parameters of all five Raman modes of UCl_3 were determined using the thermal expansion coefficient (α) of Vogel et al. (2021) and the temperature derivatives of ν_i determined in this study. The average isobaric mode Grüneisen parameter was found to be 0.91 ± 0.02. These results shed light on the U−Cl bonding behavior of UCl_3 at high temperatures and may potentially be used for modeling the speciation behavior of UCl_3 in molten salt solvents.

■ ASSOCIATED CONTENT

Supporting Information

The Supporting Information is available free of charge at https://pubs.acs.org/doi/10.1021/acs.inorgchem.3c03139.

Raman experimental setup, uncorrected Raman spectra, and calculated phonon dispersion of UCl_3 (PDF)

■ AUTHOR INFORMATION

Corresponding Author

Hongwu Xu − *Earth and Environmental Sciences Division, Los Alamos National Laboratory, Los Alamos, New Mexico 87545, United States; School of Molecular Sciences and Center for Materials of the Universe, Arizona State University, Tempe, Arizona 85287, United States;* orcid.org/0000-0002-0793-6923; Email: hxu@lanl.gov

Authors

Andrew C. Strzelecki − *Earth and Environmental Sciences Division, Los Alamos National Laboratory, Los Alamos, New Mexico 87545, United States; Materials Science Division, Los Alamos National Laboratory, Los Alamos, New Mexico 87545, United States;* orcid.org/0000-0003-3928-9422

Gaoxue Wang − *Theoretical Division, Los Alamos National Laboratory, Los Alamos, New Mexico 87545, United States;* orcid.org/0000-0003-4812-7257

Sarah M. Hickam − *Materials Science Division, Los Alamos National Laboratory, Los Alamos, New Mexico 87545, United States*

S. Scott Parker − *Materials Science Division and Sigma Division, Los Alamos National Laboratory, Los Alamos, New Mexico 87545, United States*

Rami Batrice − *Chemistry Division, Los Alamos National Laboratory, Los Alamos, New Mexico 87545, United States*

J. Matt Jackson − *Materials Science Division, Los Alamos National Laboratory, Los Alamos, New Mexico 87545, United States*

Nathan A. Conroy − *Earth and Environmental Sciences Division, Los Alamos National Laboratory, Los Alamos, New Mexico 87545, United States;* orcid.org/0000-0003-0597-3373

Jeremy N. Mitchell − *Materials Science Division, Los Alamos National Laboratory, Los Alamos, New Mexico 87545, United States*

David A. Andersson − *Materials Science Division, Los Alamos National Laboratory, Los Alamos, New Mexico 87545, United States*

Marisa J. Monreal − *Chemistry Division, Los Alamos National Laboratory, Los Alamos, New Mexico 87545, United States*

Hakim Boukhalfa − *Earth and Environmental Sciences Division, Los Alamos National Laboratory, Los Alamos, New Mexico 87545, United States*

Complete contact information is available at: https://pubs.acs.org/10.1021/acs.inorgchem.3c03139

Author Contributions

H.B., H.X., M.J.M., S.M.H., and A.C.S. designed the project. S.M.H., M.J.M., S.S.P., R.B., H.B., and A.C.S. oversaw sample preparation and characterization. *In situ* high-temperature Raman spectroscopic measurements were performed by A.C.S., with H.B. supporting the experiments. Spectral deconvolutions were performed by A.C.S. with H.B. and H.X. supporting the analyses. DFT calculations were performed by G.W. with

https://doi.org/10.1021/acs.inorgchem.3c03139
Inorg. Chem. XXXX, XXX, XXX−XXX

D.A.A. supporting the analyses. This manuscript was written through contributions of all authors. All authors have given approval to the final version of this manuscript.

Notes

The authors declare no competing financial interest.

■ ACKNOWLEDGMENTS

Research presented in this article was supported by the Laboratory Directed Research and Development (LDRD) program of Los Alamos National Laboratory (LANL) under Project 20210113DR. Computational resources were provided by the LANL Institutional Computing Program, which is supported by the U.S. Department of Energy (DOE) National Nuclear Security Administration (NNSA) under Contract 89233218CNA000001. A.C.S. acknowledges the support by the Harold Agnew National Security Postdoctoral Fellowship at LANL. The last stage of this project was also supported by the Nuclear Energy University Program (Department of Energy, DE-NE0009444). LANL, an affirmative action/equal opportunity employer, is operated by Triad National Security, LLC, for the NNSA of U.S. DOE (Contract 89233218CNA00000). LANL strongly supports academic freedom and a researcher's right to publish; as an institution, however, the Laboratory does not endorse the viewpoint of a publication or guarantee its technical correctness.

■ REFERENCES

(1) Bruno, J.; Ewing, R. C. Spent Nuclear Fuel. *Elements* **2006**, *2* (6), 343−349.
(2) Weber, W. J.; Ewing, R. C.; Vance, E. R.; Gregg, D.; Peuget, S.; Wiss, T. Plutonium in Waste Forms. In *Plutonium Handbook*; Clark, D. L., Geeson, D. A., Hanrahan, Jr., R. J., Eds.; American Nuclear Society: 2019; pp 2349−2422.
(3) Weber, W. J.; Ewing, R. C. Chapter 10: Ceramic Waste Forms for Uranium and Transuranium Elements. In *Uranium: Cradle to Grave*; Burns, P. C., Sigmon, G. E., Eds.; Mineralogical Association of Canada: 2013; pp 317−336.
(4) Strzelecki, A. C.; Bourgeois, C.; Kriegsman, K. W.; Estevenon, P.; Wei, N.; Szenknect, S.; Mesbah, A.; Wu, D.; Ewing, R. C.; Dacheux, N.; Guo, X. Thermodynamics of $CeSiO_4$: Implications for Actinide Orthosilicates. *Inorg. Chem.* **2020**, *59* (18), 13174−13183.
(5) Goel, A.; McCloy, J. S.; Pokorny, R.; Kruger, A. A. Challenges with Vitrification of Hanford High-Level Waste (HLW) to Borosilicate Glass - An Overview. *J. Non-Crystalline Solids X* **2019**, *4*, 1−19.
(6) Wegel, S.; Czempinski, V.; Oei, P.-Y.; Wealer, B. Transporting and Storing High-Level Nuclear Waste in the U.S.-Insights from a Mathematical Model. *Appl. Sci.* **2019**, *9* (12), 2437.
(7) Weber, W. J.; Navrotsky, A.; Stefanovsky, S.; Vance, E. R.; Vernaz, E. Materials Science of High-Level Immobilization. *MRS Bull.* **2009**, *34*, 46−53.
(8) McIntyre, P.; Assadi, S.; Badgley, K.; Baker, W.; Comeaux, J.; Gerity, J.; Kellams, J.; McInturff, A.; Pogue, N.; Phongikaroon, S.; Sattarov, A.; Simpson, M.; Sooby, E.; Tsvetkov, P. Accelerator-Driven Subcritical Fission in Molten Salt Core: Closing the Nuclear Fuel Cycle for Green Nuclear Energy. *AIP Conf. Proc.* **2013**, *1525* (April 2013), 636−642.
(9) Rosenthal, M. W.; Kasten, P. R.; Briggs, R. B. Molten-Salt Reactors. History, Status, and Potential. *Nucl. Appl. Technol.* **1970**, *8* (2), 107−117.
(10) Serp, J.; Allibert, M.; Beneš, O.; Delpech, S.; Feynberg, O.; Ghetta, V.; Heuer, D.; Holcomb, D.; Ignatiev, V.; Kloosterman, J. L.; Luzzi, L.; Merle-Lucotte, E.; Uhlíř, J.; Yoshioka, R.; Zhimin, D. The Molten Salt Reactor (MSR) in Generation IV: Overview and Perspectives. *Prog. Nucl. Energy* **2014**, *77*, 308−319.
(11) LeBlanc, D. Molten Salt Reactors: A New Beginning for an Old Idea. *Nucl. Eng. Des.* **2010**, *240* (6), 1644−1656.
(12) Taube, M. Fast Reactor Using Molten Chloride Salts as Fuel, Wuerenlingen, 1978.
(13) Holcomb, D. E.; Flanagan, G. F.; Patton, B. W.; Gehin, J. C.; Howard, R. L.; Harrison, T. J. Fast Spectrum Molten Salt Reactor Options, 2011.
(14) Lhermitte, C. R.; Parker, S. S.; Jackson, J. M.; Monreal, M. J. Communication—$Mg^{2+/0}$ as a Reliable Reference Electrode for Molten Chloride Salts. *J. Electrochem. Soc.* **2021**, *168* (6), 066501.
(15) Long, A. M.; Parker, S. S.; Carver, D. T.; Jackson, J. M.; Monreal, M. J.; Newmark, D. A.; Vogel, S. C. Remote Density Measurements of Molten Salts via Neutron Radiography. *J. Imaging* **2021**, *7* (5), 88.
(16) Sooby, E. S.; Nelson, A. T.; White, J. T.; McIntyre, P. M. Measurements of the Liquidus Surface and Solidus Transitions of the NaCl-UCl_3 and NaCl-UCl_3-$CeCl_3$ Phase Diagrams. *J. Nucl. Mater.* **2015**, *466*, 280−285.
(17) Parker, S. S.; Long, A.; Lhermitte, C.; Vogel, S.; Monreal, M.; Jackson, J. M. Thermophysical Properties of Liquid Chlorides from 600 to 1600 K: Melt Point, Enthalpy of Fusion, and Volumetric Expansion. *J. Mol. Liq.* **2022**, *346*, 118147.
(18) Vogel, S. C.; Andersson, D. A.; Monreal, M. J.; Jackson, J. M.; Parker, S. S.; Wang, G.; Yang, P.; Zhang, J. Crystal Structure Evolution of UCl_3 from Room Temperature to Melting. *JOM* **2021**, *73* (11), 3555−3563.
(19) Andersson, D. A.; Beeler, B. W. Ab Initio Molecular Dynamics (AIMD) Simulations of NaCl, UCl_3 and NaCl-UCl_3 Molten Salts. *J. Nucl. Mater.* **2022**, *568*, 153836.
(20) Zachariasen, W. H. Crystal Chemical Studies of the 5f-Series of Elements. I. New Structure Types. *Acta Crystallogr.* **1948**, *1* (5), 265−268.
(21) Katz, J. J.; Rabinowitch, E. *The Chemistry of Uranium, Part I: The Element, Its Binary and Related Compounds*; McGraw-Hill: New York, 1951.
(22) Strzelecki, A. C.; Reece, M. E.; Zhao, X.; Yu, W.; Benmore, C. J.; Ren, Y.; Alcorn, C. D.; Migdisov, A.; Xu, H.; Guo, X. Thermodynamics of Mixing HREE in Xenotime Solid Solution ($Er_{(x)}Yb_{(1-x)}PO_4$). *ACS Earth Sp. Chem.* **2022**, *6*, 1375.
(23) Strzelecki, A. C.; Zhao, X.; Baker, J.; Estevenon, P.; Barral, T.; Mesbah, A.; Popov, D.; Chariton, S.; Prakapenka, V.; Ahmed, S.; Yoo, C.; Dacheux, N.; Xu, H.; Guo, X. High-Pressure Structural and Thermodynamic Properties of Cerium Orthosilicates. *J. Phys. Chem. C* **2023**, *127*, 4225.
(24) Kalintsev, A.; Migdisov, A.; Alcorn, C.; Baker, J.; Brugger, J.; Mayanovic, R. A.; Akram, N.; Guo, X.; Xu, H.; Boukhalfa, H.; Caporuscio, F. A.; Viswanathan, H.; Jove-Colon, C.; Wang, Y.; Matteo, E.; Roback, R. Uranium Carbonate Complexes Demonstrate Drastic Decrease in Stability at Elevated Temperatures. *Commun. Chem.* **2021**, *4* (1), 1−8.
(25) Shapiro, S. M.; O'Shea, D. C.; Cummins, H. Z. Raman Scattering Study of the Alpha-Beta Phase Transition in Quartz. *Phys. Rev. Lett.* **1967**, *19* (7), 361−364.
(26) Heaney, P. J. Structure and Chemistry of the Low-Pressure Silica Polymorphs. In *Silica: Physical Behavior, Geochemistry, and Materials Applications*; Heaney, P. J., Prewitt, C. T., Gibbs, G. V., Eds.; De Gruyter: 1994; Vol. *29*, pp 1−40.
(27) Kresse, G.; Joubert, D. From Ultrasoft Pseudopotentials to the Projector Augmented-Wave Method. *Phys. Rev. B - Condens. Matter Mater. Phys.* **1999**, *59* (3), 1758−1775.
(28) Kresse, G.; Furthmuller, J. Efficient Iterative Schemes for Ab Initio Total-Energy Calculations Using a Plane-Wave Basis Set. *Phys. Rev. B* **1996**, *124* (20), 4053−4061.
(29) Perdew, J. P.; Burke, K.; Wang, Y. Generalized Gradient Approximation for the Exchange-Correlation Hole of a Many-Electron System. *Phys. Rev. B - Condens. Matter Mater. Phys.* **1996**, *54* (23), 16533−16539.

https://doi.org/10.1021/acs.inorgchem.3c03139
Inorg. Chem. XXXX, XXX, XXX−XXX

(30) Grimme, S. Semiempirical GGA-Type Density Functional Constructed with a Long-Range Dispersion Correction. *J. Comput. Chem.* **2006**, *27*, 1787−1799.
(31) Anisimov, V. I.; Gunnarsson, O. Density-Functional Calculation of Effective Coulomb Interactions in Metals. *Phys. Rev. B* **1991**, *43* (10), 7570−7574.
(32) Anisimov, V. I.; Zaanen, J.; Andersen, O. K. Band Theory and Mott Insulators: Hubbard U Instead of Stoner I. *Phys. Rev. B* **1991**, *44* (3), 943−954.
(33) Togo, A.; Tanaka, I. First Principles Phonon Calculations in Materials Science. *Scr. Mater.* **2015**, *108*, 1−5.
(34) Baroni, S.; de Gironcoli, S.; Dal Corso, A.; Giannozzi, P. Phonons and Related Crystal Properties from Density-Functional Perturbation Theory. *Rev. Mod. Phys.* **2001**, *73* (2), 515−562.
(35) Togo, A.; Chaput, L.; Tanaka, I.; Hug, G. First-Principles Phonon Calculations of Thermal Expansion in Ti_3SiC_2, Ti_3AlC_2, and Ti_3GeC_2. *Phys. Rev. B - Condens. Matter Mater. Phys.* **2010**, *81* (17), 1−6.
(36) Schaack, G.; Koningstein, J. A. Phonon Frequencies of Rare Earth Trichlorides with Unit Cells of Different Dimensions. *J. Phys. Chem. Solids* **1970**, *31* (11), 2417−2420.
(37) Zakir'yanova, I. D.; Salyulev, A. B. Raman Spectra of Crystalline and Molten $GdCl_3$. *Russ. Metall.* **2010**, *2010* (2), 112−115.
(38) Hawthorne, F. C.; Waychunas, G. A. Spectrum-Fitting Methods. In *Spectroscopic Methods in Mineralogy and Geology*; Hawthorne, F. C., Ed.; Mineralogical Society of America: 1988; pp 63−98.
(39) Daniel, J. F.; Wilmarth, W. R.; Begun, G. M.; Peterson, J. R. Raman Spectroscopic Studies of Gadolinium Trichloride as a Function of Temperature. *J. Crystallogr. Spectrosc. Res.* **1989**, *19* (1), 39−49.
(40) Richman, I.; Satten, R. A.; Wong, E. Y. Lattice Vibrations of $LaCl_3$ and $LaBr_3$ from Vibronic Spectra. *J. Chem. Phys.* **1964**, *40* (5), 1451−1452.
(41) Damen, T. C.; Kiel, A.; Porto, S. P. S.; Singh, S. The Raman Effects of $CeCl_3$ and $PrCl_3$. *Solid State Commun.* **1968**, *6*, 671−673.
(42) Wilmarth, W. R.; Begun, G. M.; Haire, R. G.; Young, J. P.; Peterson, J. R. The Effect of Pressure on the Raman and Absorption Spectra of $PrCl_3$, $PrBr_3$, and $NdBr_3$. *Appl. Spectrosc.* **1989**, *43* (6), 1038−1045.
(43) Wilmarth, W. R.; Begun, G. M.; Haire, R. G.; Peterson, J. R. Raman Spectra of Pm_2O_3, PmF_3, $PmCl_3$, $PmBr_3$, and PmI_3. *J. Raman Spectrosc.* **1988**, *19*, 271−275.
(44) Wilmarth, W. R.; Begun, G. M.; Haire, R. G.; Peterson, J. R. Raman Spectra of Selected Transuranium Trihalides in the Solid State. *J. Chem. Phys.* **1988**, *89* (8), 4666−4670.
(45) Del Cul, G. D.; Haire, R. G.; Peterson, J. R. Effects of Pressure on the Luminescence, Raman and Absorption Spectra of $^{248}CmCl_3$. *J. Alloys Compd.* **1992**, *181* (1−2), 63−70.
(46) Zakir'yanova, I. D.; Salyulev, A. B.; Khokhlov, V. A. Raman Spectroscopy Study of the Phase Transitions in Rare-Earth Metal Trichlorides. *Russ. Metall.* **2011**, *2011* (8), 754−759.
(47) Tuffy, B. W.; Birkner, N. R.; Schorne-pinto, J.; Davis, R. C.; Mofrad, A. M.; Dixon, C. M.; Aziziha, M.; Christian, M. S.; Lynch, T. J.; Bartlett, M. T.; Besmann, T. M.; Brinkman, K. S.; Chiu, W. K. S. Identification and Decomposition of Uranium Oxychloride Phases in Oxygen-Exposed UCl_3 Salt Compositions. *J. Phys. Chem. B* **2023**, *127*, 6091.
(48) Spano, T. L.; Olds, T. A.; McDonnell, M.; Smith, R.; Niediela, J. L.; Miskowiec, A.; Kapsimalis, R.; Shields, A. A. CURIES: Compednium of Uranium Raman and Infrared Experimental Spectra. *Am. Mineral.* **2023**, DOI: 10.2138/am-2022-8738, in press.
(49) Karcher, S.; Mohun, R.; Olds, T. A.; Weber, M.; Kriegsman, K.; Zhao, X.; Guo, X.; Corkhill, C.; Field, D.; McCloy, J. Benefits of Using Multiple Raman Laser Wavelengths for Characterizing Defects in a UO_2 Matrix. *J. Raman Spectrosc.* **2022**, *53* (5), 988−1002.
(50) Olds, T. A.; Karcher, S. E.; Kriegsman, K. W.; Guo, X.; McCloy, J. S. Oxidation and Anion Lattice Defect Signatures of Hypostoichiometric Lanthanide-Doped UO_2. *J. Nucl. Mater.* **2020**, *530*, 151959.
(51) Anderson, O. L. *Equations of State of Solids for Geophysics Ceramic Science*; Charnock, H., Dewey, J., Morris, S. C., Navrotsky, A., Oxburgh, E. R., Price, R. A., Skinner, B. J., Eds.; Oxford University Press: 1995; Vol. *31*.
(52) Carter, R. L. Vibrational Spectroscopy. In *Molecular Symmetry and Group Theory*; Wiley: 1997; pp 164−200.
(53) Navrotsky, A. Systematic Trends and Prediction of Enthalpies of Formation of Refractory Lanthanide and Actinide Ternary Oxide Phases. *Ceram. Trans.* **2001**, No. 119, 137−146.
(54) Helean, K. B.; Navrotsky, A.; Lumpkin, G. R.; Colella, M.; Lian, J.; Ewing, R. C.; Ebbinghaus, B.; Catalano, J. G. Enthalpies of Formation of U-, Th-, Ce-Brannerite: Implications for Plutonium Immobilization. *J. Nucl. Mater.* **2003**, *320* (3), 231−244.
(55) Navrotsky, A. Thermochemical Insights into Refractory Ceramic Materials Based on Oxides with Large Tetravalent Cations. *J. Mater. Chem.* **2005**, *15* (19), 1883−1890.
(56) Qi, J.; Guo, X.; Mielewczyk-Gryn, A.; Navrotsky, A. Formation Enthalpies of $LaLnO_3$ (Ln = Ho, Er, Tm and Yb) Interlanthanide Perovskites. *J. Solid State Chem.* **2015**, *227*, 150−154.
(57) Helean, K. B.; Ushakov, S. V.; Brown, C. E.; Navrotsky, A.; Lian, J.; Ewing, R. C.; Farmer, J. M.; Boatner, L. A. Formation Enthalpies of Rare Earth Titanate Pyrochlores. *J. Solid State Chem.* **2004**, *177* (6), 1858−1866.
(58) Guo, X.; Tiferet, E.; Qi, L.; Solomon, J. M.; Lanzirotti, A.; Newville, M.; Engelhard, M. H.; Kukkadapu, R. K.; Wu, D.; Ilton, E. S.; Asta, M.; Sutton, S. R.; Xu, H.; Navrotsky, A. U(v) in Metal Uranates: A Combined Experimental and Theoretical Study of $MgUO_4$, $CrUO_4$, and $FeUO_4$. *Dalt. Trans.* **2016**, *45* (11), 4622−4632.
(59) Chen, F.; Ewing, R. C.; Clark, S. B. The Gibbs Free Energies and Enthalpies of Formation of U^{6+} Phases: An Empirical Method of Prediction. *Am. Mineral.* **1999**, *84* (4), 650−664.
(60) Sverjensky, D.; Shock, E. L.; Helgeson, H. C. Prediction of the Thermodynamic Properties of Aqueous Metal Complexes to 1000 C and 5 Kb. *Geochim. Cosmochim. Acta* **1997**, *61* (7), 1359−1412.
(61) Anderson, D. L.; Anderson, O. L. The Bulk Modulus-Volume Relationship for Oxides. *J. Geophys. Res.* **1970**, *75* (17), 3494−3500.
(62) Xu, H.; Zhao, Y.; Zhang, J.; Wang, Y.; Hickmott, D. D.; Daemen, L. L.; Hartl, M. A.; Wang, L. Anisotropic Elasticity of Jarosite: A High-P Synchrotron XRD Study. *Am. Mineral.* **2010**, *95* (1), 19−23.
(63) Harris, D. C.; Bertolucci, M. D. *Symmetry and Spectroscopy: An Introduction to Vibrational and Electronical Spectroscopy*; Oxford University Press: 1978.
(64) Bishop, D. M. Molecular Vibrations. In *Group Theory and Chemistry*; Clarendon Press: 1973; pp 164−195.
(65) Shannon, R. D. Revised Effective Ionic Radii and Systematic Studies of Interatomic Distances in Halides and Chalcogenides. *Acta Crystallogr., Sect. A* **1976**, *32* (5), 751−767.
(66) Lundberg, D.; Persson, I. The Size of Actinoid (III) Ions - Structural Analysis vs. Common Misinterpretations. *Coord. Chem. Rev.* **2016**, *318*, 131−134.
(67) Momma, K.; Izumi, F. VESTA 3 for Three-Dimensional Visualization of Crystal, Volumetric and Morphology Data. *J. Appl. Crystallogr.* **2011**, *44* (6), 1272−1276.

https://doi.org/10.1021/acs.inorgchem.3c03139
Inorg. Chem. XXXX, XXX, XXX−XXX